IEEE Robotics and Automation Letters (RA-L) paper, presented at ICRA 2026, Vienna, Austria. Cite as RA-L paper.

Tightly Coupled Rao-Blackwellized Particle Filter for GNSS-Only Positioning in Urban Environments Without Ambiguity Resolution

Daiki Niimi[1], An Fujino[1], Taro Suzuki[2], and Junichi Meguro[3]

***Abstract*—This paper presents a tightly coupled Rao-Blackwellized particle filter (TC-RBPF) for global navigation satellite system (GNSS) positioning that eliminates the need for carrier-phase integer ambiguity resolution. The previously proposed loosely coupled RBPF (LC-RBPF) approach uses carrier-phase residuals to estimate particle likelihoods, enabling positioning without integer ambiguity resolution. However, the position estimation accuracy depends on the performance of the state transition. The previous approach estimates velocity using a Kalman filter (KF) based on least-squares Doppler measurements, which are vulnerable to non-line-of-sight (NLOS) multipath errors. This often leads to complete positioning failure in urban environments. To overcome these limitations, the proposed TC-RBPF tightly integrates raw Doppler measurements into the KF. This enables consistent estimation of both velocity and receiver clock drift within a time-series framework. Furthermore, a robust KF based on Student's t-distribution and particle-wise NLOS rejection using double-differenced pseudorange residuals are introduced to mitigate the impact of outliers. Together, these mechanisms enhance outlier robustness and transition reliability. Experimental evaluations in six challenging urban scenarios demonstrate that the proposed method achieves superior positioning performance compared to existing methods, confirming its effectiveness under degraded GNSS conditions.**

***Index Terms*—Localization, Autonomous Vehicle Navigation, Probability and Statistical Methods, GNSS, RBPF.**

I. Introduction

GLOBAL navigation satellite system (GNSS) has become an indispensable component for localization of outdoor mobile robots due to its unique ability to estimate absolute positions on Earth. In particular, real-time kinematic (RTK) GNSS realizes real-time centimeter-level positioning accuracy by precisely resolving integer ambiguities contained in the double-differenced (DD) carrier-phase observations. Owing to this capability, RTK-GNSS is widely adopted in applications such as autonomous vehicles, for which a localization accuracy of around 0.3 meters is regarded as essential [1]. However, integer ambiguity resolution can become unstable under multipath conditions, particularly in urban environments where non-line-of-sight (NLOS) multipath signals are a major source of GNSS positioning errors, often resulting in incorrect integer ambiguity estimates [2]. This significantly degrades RTK-GNSS positioning accuracy. Furthermore, urban environments often cause GNSS signal blockages and cycle slips, which interrupt carrier-phase continuity and require frequent re-resolution of integer ambiguities [3]. As a result, it becomes difficult to maintain continuous high-precision positioning.

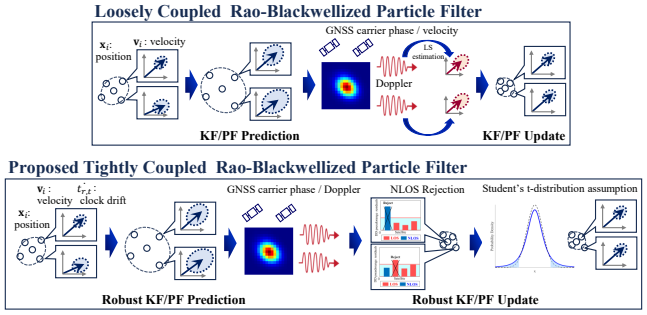

Fig. 1. Overview of the proposed TC-RBPF. Top: The LC-RBPF estimates velocity using a KF with LS-estimated Doppler velocity. Bottom: The proposed TC-RBPF directly incorporates raw Doppler measurements into the KF, augments the state with receiver clock drift, and introduces NLOS rejection and a Student's t-based robust KF for enhanced robustness.

In contrast, alternative GNSS positioning approaches have been proposed that eliminate the need for integer ambiguity resolution [4]. The previous study [5] developed a particle filter (PF)-based method that utilizes the residuals of carrier-phase observations to compute particle likelihoods. This approach enables the method to achieve positioning accuracy comparable to that of RTK-GNSS, without requiring integer ambiguity resolution. However, the accuracy of PF-based methods fundamentally depends on the reliability of the state transition, as particles must be distributed around the true state to enable accurate likelihood computation. In the PF, the state transition is performed using velocity estimated via least-squares (LS) from GNSS Doppler measurements. However, urban environments introduce significant multipath errors into Doppler-based velocity estimation, making the method vulnerable to degraded transitions and eventual PF failure in challenging scenarios [6].

To address these issues, the previous study [7] further extended the PF framework using Rao-Blackwellization, allowing velocity estimation through a Kalman filter (KF) without increasing the dimensionality of the PF. This enhancement allows the method to achieve even higher positioning accuracy than RTK-GNSS. However, in the Rao-Blackwellized PF (RBPF), the KF is implemented in a loosely coupled (LC) framework, in which the 3D velocity observations are ob-

Manuscript received: August 10, 2025; Revised: November 7, 2025; Accepted: November 12, 2025.

This paper was recommended for publication by Editor Soon-Jo Chung upon evaluation of the Associate Editor and Reviewers' comments.

[1]Daiki Niimi and An Fujino are with the Division of Mechatronics Engineering, Graduate School of Science and Technology, Meijo University, 1-501 Shiogamaguchi, Tempaku-ku, Nagoya, Aichi 468-8502, Japan. {243432020, 210447077}@ccmailg.meijo-u.ac.jp

[2]Taro Suzuki is with the Future Robotics Technology Center (fuRo), Chiba Institute of Technology, Tsudanuma 2-17-1, Narashino, Chiba 275-0016, Japan. taro@furo.org

[3]Junichi Meguro is with the Department of Mechatronics Engineering, Faculty of Science and Technology, Meijo University, 1-501 Shiogamaguchi, Tempaku-ku, Nagoya, Aichi 468-8502, Japan. meguro@meijo-u.ac.jp

Digital Object Identifier (DOI): see top of this page.

IEEE Robotics and Automation Letters (RA-L) paper, presented at ICRA 2026, Vienna, Austria. Cite as RA-L paper.

tained via LS estimation from GNSS Doppler measurements. Although this approach improves robustness compared to the original PF, it does not fundamentally resolve the limitations of Doppler-based velocity estimation under severe multipath conditions. As a result, the positioning accuracy of the RBPF degrades in more challenging urban environments.

Therefore, this study proposes a tightly coupled (TC) RBPF that enables centimeter-level positioning accuracy without requiring integer ambiguity resolution and enhances robustness in harsh urban environments. Fig. 1 shows an overview of the proposed TC-RBPF. The proposed method extends the RBPF framework to a tightly coupled formulation, where raw Doppler measurements are directly incorporated into the KF as observations. This formulation enables continuous velocity estimation even in environments with a limited number of visible satellites. However, the accuracy of the velocity estimation can be severely degraded if the filter incorporates erroneous Doppler measurements from even a single satellite affected by multipath. To reject or mitigate the influence of these outliers, the proposed method introduces two key components: an NLOS rejection scheme based on DD pseudorange residuals at each particle's position, and a robust KF based on Student's t-distribution. Consequently, the proposed method achieves robust position estimation in harsh urban environments, such as those with few visible satellites or frequent multipath conditions.

II. Related Work

A. GNSS integer ambiguity resolution

In standard RTK-GNSS, float ambiguities are initially estimated using a KF. Subsequently, integer ambiguities are resolved using an integer LS method, such as the LAMBDA method [4], [8], [9]. Once integer ambiguities are correctly fixed, centimeter-level positioning accuracy can be achieved. However, multipath effects can prevent ambiguity resolution for certain satellites, leading to a significant degradation in positioning accuracy [10]. In addition, cycle slips can disrupt carrier-phase continuity, requiring re-initialization of the ambiguity resolution process. To address these challenges, various techniques, such as partial ambiguity resolution and NLOS detection, have been proposed [2], [11]–[13]. However, whether it is possible to accurately identify satellites with unresolved ambiguities or affected by NLOS, and to completely eliminate the impact of multipath using GNSS-only information remains an open question.

In contrast, the ambiguity function method (AFM) [14] and its improved version, the modified AFM (MAFM) [15]–[17], have been proposed. These methods utilize an ambiguity function value (AFV), defined on the basis of fractional carrier-phase measurements, to quantify the deviation of ambiguities from integers. Consequently, the location that minimizes the AFV evaluated on the candidate positions in a 3D space corresponds to the optimal position. These methods achieve robustness against cycle slips through the avoidance of explicit ambiguity resolution. However, their high computational cost is a significant drawback, limiting their practicality. To address this, the previous study [5] proposed a positioning method that combines AFM with a PF. Instead of explicitly resolving integer ambiguities using AFV, this approach evaluates AFV as the likelihood of each particle. However, since this method computes likelihoods based on particle position hypotheses, it can fail if the particles do not adequately track the true position.

B. Rao-Blackwellized PF

The RBPF, also known as the marginalized PF, takes advantage of the structure of the state space by factorizing the joint distribution into a nonlinear component, estimated by a PF, and a conditionally linear component, estimated using a KF or another Bayesian filter [18], [19]. In standard PFs, as the state dimensionality increases, the number of required particles grows exponentially, significantly increasing the computational cost. This problem is widely known as the curse of dimensionality [20], [21]. In contrast, this decomposition enables accurate estimation without increasing the computational burden associated with high-dimensional PFs, making the RBPF particularly suitable for state estimation problems involving high-dimensional states. RBPF is employed in various fields to address state estimation problems [22]. In the field of robotics and automation, RBPFs have been widely adopted in simultaneous localization and mapping (SLAM) [23]–[25]. Beyond SLAM, they have also been utilized in frameworks that integrate GNSS, inertial navigation systems (INS) and cameras [26], [27]. Although PF-based methods have been proposed that combine GNSS with 3D maps [28]–[30], RBPF has not been employed in these settings, and GNSS-only applications remain underexplored. This is largely because GNSS-based positioning has traditionally been handled with relatively linear models, for which Bayesian filters such as KF have been considered sufficient, reducing the perceived need for PF.

In contrast, the previous work [5] employs AFM, which requires evaluating multiple position hypotheses to estimate the final position. Since this process inherently relies on particle-based sampling, it can only be realized using a PF. Based on this idea, the LC-RBPF [7] was previously proposed in which the 3D position is estimated using a PF, while the 3D velocity is estimated using a KF. In this framework, the AFV is used as the observation model for the nonlinear state (position), and the velocity estimated via LS from GNSS Doppler measurements serves as the observation for the linear state (velocity). The improved velocity estimates provided by the KF contribute to more accurate state transitions in the PF, leading to enhanced overall positioning performance. However, this approach still relies on Doppler velocities computed via LS, which are sensitive to multipath effects. In more severe urban conditions, this sensitivity can degrade the robustness of velocity estimation and, consequently, the reliability of the entire RBPF framework.

C. Contributions

The contributions of this study are delineated as follows.

- This is the first study to introduce a TC-RBPF for GNSS-only positioning, enabling simultaneous estimation of

IEEE Robotics and Automation Letters (RA-L) paper, presented at ICRA 2026, Vienna, Austria. Cite as RA-L paper.

3D position, velocity and receiver clock drift with high accuracy.

- Tightly integrating Doppler observations into the KF improves velocity estimation accuracy, which in turn enhances both the state transition performance of the PF and the quality of likelihood evaluation, without relying on integer ambiguity resolution.
- The proposed method enhances the reliability of the entire RBPF framework by introducing a PF-based NLOS rejection scheme and a Student's t-based KF, allowing robust velocity estimation in the presence of outliers.
- The effectiveness of the proposed method is validated using real-world data from multiple challenging urban environments, demonstrating improved positioning accuracy compared to existing methods.

III. Proposed Method

This study proposes a TC-RBPF that extends the previously developed LC-RBPF. Specifically, Doppler measurements are directly incorporated as observations in the KF, allowing the RBPF to jointly estimate 3D position, 3D velocity, and receiver clock drift. This tight integration improves the robustness of the velocity estimation, which in turn enhances the state transition performance of the PF.

A. Rao-Blackwellization

The state at time t is denoted as $\mathbf{x}_t$, which consists of a nonlinear component $\mathbf{x}_t^n$ and a linear component $\mathbf{x}_t^l$. Given the sequence of observations $\mathbf{y}_{0:t}$, the joint posterior distribution can be factorized under the Rao-Blackwellization framework as follows:

$$\begin{aligned} p\left(\mathbf{x}_t \mid \mathbf{y}_{0:\,t}\right) &= p\left(\mathbf{x}_t^l, \mathbf{x}_{0:\,t}^n \mid \mathbf{y}_{0:\,t}\right) \\ &= p\left(\mathbf{x}_{0:\,t}^n \mid \mathbf{y}_{0:\,t}\right) p\left(\mathbf{x}_t^l \mid \mathbf{x}_{0:\,t}^n, \mathbf{y}_{0:\,t}\right) \end{aligned} \tag{1}$$

As shown in (1), Rao-Blackwellization enables the decomposition of the joint posterior into a marginal distribution over the nonlinear state and a conditional distribution over the linear state given the nonlinear state. In this study, the marginal distribution of the nonlinear state $p\left(\mathbf{x}_{0:t}^n \mid \mathbf{y}_{0:t}\right)$ is estimated using a PF, while the conditional distribution of the linear state given each particle $p\left(\mathbf{x}_t^l \mid \mathbf{x}_{0:t}^n, \mathbf{y}_{0:t}\right)$ is estimated using a KF. This study defines the nonlinear state $\mathbf{x}_t^n$ as the 3D position, and the linear state $\mathbf{x}_t^l$ as the 3D velocity $\mathbf{v}_t$ and the receiver clock drift $\dot{t}_{r,t}$.

$$\mathbf{x}_t^l = \begin{bmatrix} \mathbf{v}_t \\ \dot{t}_{r,t} \end{bmatrix} \tag{2}$$

The time step is denoted by Δt. The process noise terms for the nonlinear and linear states are represented by $\mathbf{w}_t^n$ and $\mathbf{w}_t^l$, respectively, and the observation noise is denoted by $\mathbf{e}_t$. The linear observation matrix is given by $\mathbf{C}_t$, and the observation function is denoted by $h(\cdot)$. Based on these definitions, the state transition and observation models are formulated as follows:

$$\mathbf{x}_{t+1}^n = \mathbf{x}_t^n + \Delta t \mathbf{v}_t + \mathbf{w}_t^n \tag{3}$$

Algorithm 1 Proposed TC-RBPF algorithm for one epoch

1) PF Prediction
Predict particle position (3)
2) KF Time Update
- Predict velocity/clock drift (9)
- Predict error covariance (10)
3) PF Correction
Calculate DD residuals
- DD pseudorange residuals (6)
- AFV (7)
Calculate likelihood (8) / Resampling
4) NLOS Detection
Detect NLOS using DD pseudorange residuals (15)
5) KF Measurement Update
- Update velocity/clock drift (16)
- Update error covariance (17)

$$\mathbf{x}_{t+1}^l = \mathbf{x}_t^l + \mathbf{w}_t^l \tag{4}$$

$$\mathbf{y}_t = h(\mathbf{x}_t^n) + \mathbf{C}_t \mathbf{x}_t^l + \mathbf{e}_t \tag{5}$$

In the proposed method, the position is updated using (3), while velocity and receiver clock drift are updated using (4). As shown in (5), the RBPF framework conditions the estimation of the linear state $\mathbf{x}_t^l$ (3D velocity and receiver clock drift) on the nonlinear state $\mathbf{x}_t^n$ (3D position), such that the position influences their estimation through the observation model. This structure allows the diversity of position hypotheses, represented by particles, to propagate into the linear state estimation, enabling the RBPF to capture a richer posterior over the full state space.

The algorithm 1 outlines the proposed TC-RBPF framework for one epoch. The key features of the proposed method lie in the likelihood evaluation within the PF and the velocity estimation using the KF.

B. Likelihood evaluation in PF

To estimate the position with centimeter-level accuracy, the proposed method adopts the likelihood evaluation scheme from the previous study [5]. The likelihood is evaluated on the basis of DD pseudorange and carrier-phase residuals at each particle position, eliminating the need for integer ambiguity resolution. Within this framework, the final position is estimated through multiple updates of likelihood evaluation and resampling. Refer to paper [5] for details on the procedure for multiple updates.

1) Pseudorange Residuals: Pseudorange measurements provide ambiguity-free information. Since the DD pseudorange has already eliminated the satellite and receiver clock, as well as the ionospheric and tropospheric delays, it can be expressed solely in terms of the DD geometric distance between the satellite and the receiver. Consequently, the DD pseudorange residual $\delta_\rho(\rho^k, \mathbf{x}_i^n)$ for the k-th measurement at the 3D position $\mathbf{x}_i^n$ of the i-th particle is computed as the

IEEE Robotics and Automation Letters (RA-L) paper, presented at ICRA 2026, Vienna, Austria. Cite as RA-L paper.

difference between the DD pseudorange ρ^k and the DD geometric distance $r^k(\mathbf{x}_i^n)$ between the satellite and the particle.

$$\delta_\rho(\rho^k, \mathbf{x}_i^n) = \rho^k - r^k(\mathbf{x}_i^n) \tag{6}$$

2) Carrier-phase Residuals: Carrier-phase measurements contain integer ambiguity terms. Therefore, the DD carrier-phase includes not only the DD geometric distance but also the DD integer ambiguity term. Since the integer ambiguity is an unknown parameter, it must be resolved to utilize the measurement effectively. However, ambiguity resolution is often challenged by issues such as cycle slips, as discussed in Section II. To address this, the proposed method evaluates the likelihood of particles using the AFV. Given the DD carrier-phase Φ^k for the k-th measurement and the carrier wavelength λ, the AFV at the particle position $\mathbf{x}_i^n$ is calculated by the following equation [14].

$$\delta_\Phi\left(\Phi^k, \mathbf{x}_i^n\right) = \text{round}\left(\Phi^k - \frac{1}{\lambda} r^k\left(\mathbf{x}_i^n\right)\right) - \left(\Phi^k - \frac{1}{\lambda} r^k\left(\mathbf{x}_i^n\right)\right) \tag{7}$$

The operator $\text{round}(\cdot)$ denotes the rounding to the nearest integer. In the given (7), the effect of the integer ambiguity is removed, allowing focus on the fractional part of the carrier-phase measurement. The AFV evaluates how far the ambiguity deviates from an integer value at each particle position. If a particle is located at the true position, the corresponding ambiguity becomes an integer, resulting in an AFV of zero. Conversely, the farther the particle is from the true position, the larger the AFV becomes.

3) Likelihood Estimation: Both pseudorange and carrier-phase residuals are incorporated into the PF using a unified likelihood model. Let $\delta^k\left(\mathbf{x}_i^n\right)$ denote the DD residual of the GNSS observation at the position $\mathbf{x}_i^n$ of the i-th particle. This term corresponds to either the DD pseudorange residual $\delta_\rho(\rho^k, \mathbf{x}_i^n)$ or the AFV $\delta_\Phi(\Phi^k, \mathbf{x}_i^n)$, depending on the type of observation used. The likelihood is then computed as:

$$p\left(\delta\left(\mathbf{x}_i^n\right)\right) = \frac{1}{\sqrt{2\pi}\sigma} \prod_{k=1}^{K} \exp\left(-\frac{\delta^k\left(\mathbf{x}_i^n\right)^2}{2\sigma^2}\right) \tag{8}$$

The parameter σ denotes the standard deviation of the measurement noise, which is set at 2.0 meters for DD pseudorange residuals and 0.2 cycles for the AFV in this study. As shown in (8), the final likelihood is calculated by aggregating the likelihoods across multiple satellites and frequency bands. This aggregation suppresses the periodic multiple peaks inherent to carrier-phase measurements and mitigates the risk of convergence to incorrect peaks.

Fig. 2 illustrates the likelihoods computed using (8) based on the AFV obtained from (7) and their corresponding satellite sky plots. The AFV is computed using dual-frequency (L1 and L2) carrier-phase measurements from GPS, Galileo, BeiDou, and QZSS satellites over a ± 1 meter area centered at the true position with 0.01 meter grid intervals. Two environments are considered: open-sky and urban. The left panels depict the open-sky case, where 15 well-distributed satellites yield a sharp, single likelihood peak. In contrast, the right panels

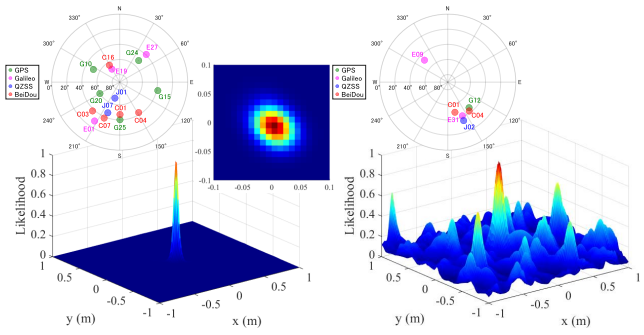

Fig. 2. Example of likelihoods computed from AFV and their corresponding satellite sky plots. Left (open-sky): The likelihood shows a single, sharp peak, which is the result of the 15 well-distributed satellites. Right (urban): The likelihood shows multiple peaks, caused by signal blockage that reduces visible satellites to 6.

correspond to an urban scenario in which signal blockage reduces visible satellites to 6. This reduction in the number of satellites is the primary factor causing the likelihood degradation. Specifically, this small number of satellites is insufficient for the aggregation process to effectively suppress the periodic ambiguity peaks inherent in the AFV, resulting in multiple false peaks. Therefore, it is crucial for the particles to be near the true position, especially in urban environments, to prevent convergence to false likelihood peaks.

C. Velocity estimation using robust KF

The proposed method adopts a framework in which Doppler measurements are directly used as observations in a KF to estimate velocity, enabling statistical treatment of observation errors from each satellite within the filter. To mitigate the effects of outliers and multipath, the proposed method employs a robust KF in conjunction with NLOS satellite exclusion, where satellites affected by NLOS multipath are explicitly removed and observation weights are adjusted according to their reliability. This approach enables accurate velocity estimation even in challenging urban environments. In the proposed TC-RBPF, the robust KF estimates the state using a standard two-step procedure consisting of a time update and a measurement update.

1) Time update: The time update step is performed using the following equations.

$$\hat{\mathbf{x}}_{t+1|t}^l = \bar{\mathbf{A}}_t^l \mathbf{x}_{t|t}^l + \mathbf{L}_t \begin{bmatrix} \left(\hat{\mathbf{x}}_{t+1|t}^n - \mathbf{x}_{t|t}^n\right) - \mathbf{A}_t^n \mathbf{v}_{t|t} \\ \xi_t \end{bmatrix} \tag{9}$$

$$\hat{\mathbf{P}}_{t+1|t} = \bar{\mathbf{A}}_t^l \mathbf{P}_{t|t} \left(\bar{\mathbf{A}}_t^l\right)^T + \mathbf{Q}_t^l - \mathbf{L}_t \mathbf{N}_t \mathbf{L}_t^T \tag{10}$$

Here, $\bar{\mathbf{A}}_t^l$ and $\mathbf{A}_t^n$ denote the state transition matrices for the linear and nonlinear states, respectively, while $\mathbf{Q}_t^l$ and $\mathbf{Q}_t^n$ are the corresponding process noise covariance matrices. The term $\boldsymbol{\xi}_t$ represents Brownian noise added to the receiver clock drift component of the linear state, modeling its process uncertainty. In addition, $\mathbf{L}_t$ and $\mathbf{N}_t$ are defined as follows:

$$\mathbf{L}_t = \bar{\mathbf{A}}_t^l \mathbf{P}_{t|t} \left(\mathbf{A}_t^n\right)^T \mathbf{N}_t^{-1} \tag{11}$$

IEEE Robotics and Automation Letters (RA-L) paper, presented at ICRA 2026, Vienna, Austria. Cite as RA-L paper.

$$\mathbf{N}_t = \mathbf{A}_t^n \mathbf{P}_{t|t} \left(\mathbf{A}_t^n\right)^T + \mathbf{Q}_t^n \tag{12}$$

In (9), the term $\left(\hat{\mathbf{x}}_{t+1}^n - \mathbf{x}_t^n\right) - \mathbf{A}_t^n \mathbf{x}_{t|t}^l$ represents the difference between the actual change in position resulting from the PF's state transition and the predicted change based on the previously estimated velocity. This residual captures particle-specific position deviations caused by noise introduced during the PF's transition step. As a result, velocity noise can be dynamically determined from the actual position change, enabling adaptive modeling of motion uncertainty.

2) Measurement update: To estimate receiver velocity $\mathbf{v}_t$ and receiver clock drift $\dot{t}_{r,t}$, Doppler measurements are directly used as observations in the KF. Let D_t^k denote the Doppler observation of the k-th satellite at time t, $\mathbf{v}_{s,t}^k$ the satellite velocity, $\mathbf{u}_t^k$ the LOS unit vector from the receiver to the satellite and $\dot{t}_{s,t}^k$ the satellite clock drift. The Doppler shift model is expressed as:

$$\lambda D_t^k = (\mathbf{v}_{s,t}^k - \mathbf{v}_t) \cdot \mathbf{u}_t^k + (\dot{t}_{r,t} - \dot{t}_{s,t}^k) + \epsilon_D \tag{13}$$

Rearranging (13), the Doppler residual is calculated using the following equation.

$$\delta_D = (\lambda D_t^k - \mathbf{v}_{s,t}^k \cdot \mathbf{u}_t^k + \dot{t}_{s,t}^k) - (-\mathbf{v}_t \cdot \mathbf{u}_t^k + \dot{t}_{r,t}) \tag{14}$$

Based on (14), the KF is formulated by treating the Doppler residual as the innovation for the linear state update. This model is extended to all observable satellites at each time step, forming a stacked observation vector and the corresponding design matrix for use in the KF update. This formulation allows for finer-grained handling of satellite-wise observation quality and enables more accurate and responsive velocity estimation, particularly in challenging environments. However, to achieve high-precision velocity estimation, it is essential to incorporate a mechanism that reduces or completely rejects the influence of poor measurements on the final state estimate.

Therefore, the proposed method rejects NLOS Doppler measurements using the DD pseudorange residuals. Specifically, NLOS satellites are identified and removed by thresholding DD pseudorange residuals, which are computed for each particle's position according to (6).

$$\mathrm{abs}\left(\delta_\rho(\rho^k, \mathbf{x}_i^n)\right) > \zeta \tag{15}$$

Here, ζ is an empirically determined threshold. This approach allows each particle to independently reject NLOS satellites based on its position-dependent residuals. Consequently, particles closer to the true position are more likely to estimate velocity using reliable satellite subsets, improving overall estimation accuracy. However, this method does not completely eliminate the influence of all poor-quality measurements.

To further mitigate the impact of outliers not detected by the NLOS rejection process, the proposed method employs a robust KF based on the Student's t-distribution [31], [32]. GNSS observation errors often exhibit heavy-tailed characteristics as a result of multipath and other non-Gaussian effects. The Student's t-based KF addresses this by adaptively down-weighting such measurements during the update step. The measurement update in this formulation is performed as follows:

$$\mathbf{x}_{t|t}^l = \hat{\mathbf{x}}_{t|t-1}^l + \mathbf{K}_t \left(\mathbf{y}_t - \begin{bmatrix} h(\mathbf{x}_t^n) \\ \mathbf{C}_t \hat{\mathbf{x}}_{t|t-1}^l \end{bmatrix} \right) \tag{16}$$

$$\mathbf{P}_{t|t} = \hat{\mathbf{P}}_{t|t-1} - \mathbf{K}_t \mathbf{M}_t \mathbf{K}_t^T \tag{17}$$

where $\mathbf{K}_t$ and $\mathbf{M}_t$ are defined as follows:

$$\mathbf{K}_t = \hat{\mathbf{P}}_{t|t-1} \mathbf{C}_t^T \mathbf{M}_t^{-1} \tag{18}$$

$$\mathbf{M}_t = \mathbf{C}_t \hat{\mathbf{P}}_{t|t-1} \mathbf{C}_t^T + \frac{\nu + \boldsymbol{\Delta}_t^2}{\nu + d} \mathbf{R}_t \tag{19}$$

$$\boldsymbol{\Delta}_t = \sqrt{\left(\mathbf{y}_t - h(\mathbf{x}_t^n) - \mathbf{C}_t \hat{\mathbf{x}}_{t|t-1}^l\right)^T \mathbf{M}_t \left(\mathbf{y}_t - h(\mathbf{x}_t^n) - \mathbf{C}_t \hat{\mathbf{x}}_{t|t-1}^l\right)} \tag{20}$$

In (19), $\mathbf{R}_t$ is the nominal observation noise covariance matrix. It is determined using a standard weighting model from [33] that computes a variance multiplier based on the satellite's elevation angle and carrier-to-noise density ratio (C/N0). This mechanism inflates the variance for low-quality signals, thereby down-weighting them in the filter update. Furthermore, $\boldsymbol{\Delta}_t$ denotes the Mahalanobis distance of the innovation, as defined in (20), where d is the dimension of the innovation vector and ν is the degrees-of-freedom parameter of the Student's t-distribution. The scaling factor $\frac{\nu+\boldsymbol{\Delta}_t^2}{\nu+d}$ increases the effective covariance of the observation noise when the innovation is large, which typically indicates an outlier. As a result, the influence of such outliers on the state update is reduced, enhancing the robustness of the filter.

In (16), the innovation term $\mathbf{y}_t - \begin{bmatrix} h(\mathbf{x}_t^n) & \mathbf{C}_t \hat{\mathbf{x}}_{t|t-1}^l \end{bmatrix}^T$ includes the effects of nonlinear components $h(\mathbf{x}_t^n)$, allowing the velocity estimate to be updated using both linear and nonlinear observations. For the linear observation, the proposed method utilizes Doppler measurements from particle-specific reliable satellite sets constructed according to (15). For the nonlinear observation, $h(\mathbf{x}_t^n)$ cannot be computed directly. Instead, employing the AFV as the innovation term $\mathbf{y}_t - h(\mathbf{x}_t^n)$ enables its evaluation.

IV. Evaluation Experiment

A. Setup

To evaluate the effectiveness of the proposed method, experiments were conducted using the PPC Dataset [34] collected in six urban environments in Nagoya and Tokyo, Japan, with a vehicle. GNSS data were acquired using a Septentrio mosaic-X5 receiver, utilizing signals from the GPS, Galileo, BeiDou, and QZSS constellations. The environments used in this evaluation are illustrated in Fig. 3, where the color along each trajectory represents the number of visible satellites observed at each location.

Estimation performance was evaluated using three accuracy metrics. To assess the quality of the state transition in the PF, the velocity estimation accuracy was evaluated using the cumulative distribution function (CDF) of velocity errors,

IEEE Robotics and Automation Letters (RA-L) paper, presented at ICRA 2026, Vienna, Austria. Cite as RA-L paper.

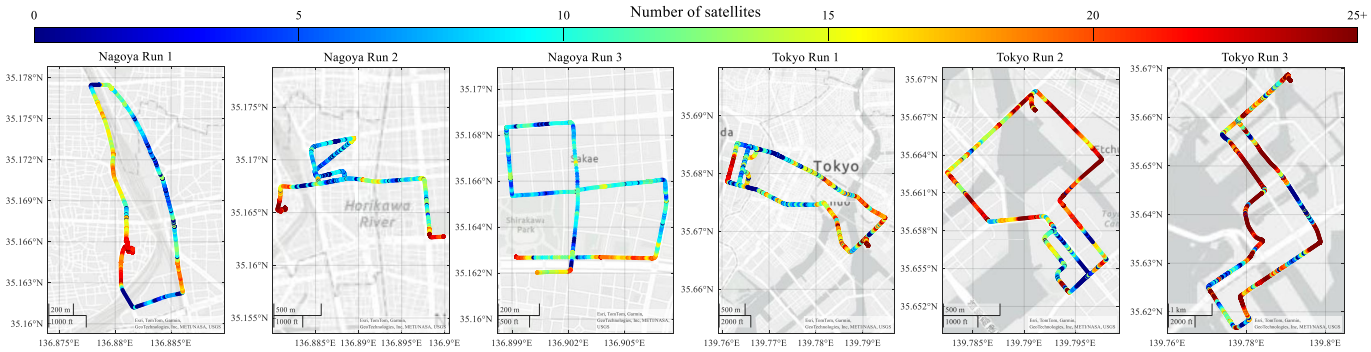

Fig. 3. Evaluation environments in Nagoya and Tokyo, Japan. Trajectory colors indicate the number of visible satellites, with warmer colors representing higher counts. The dataset covers diverse urban conditions for GNSS performance evaluation.

TABLE I
STATE TRANSITION PERFORMANCE COMPARISON OF EACH METHOD ACROSS SIX TEST RUNS.

Method	Nagoya Run1		Nagoya Run2		Nagoya Run3		Tokyo Run1		Tokyo Run2		Tokyo Run3	
	CDF $\leq$ 0.1 m/s	Within peak	CDF $\leq$ 0.1 m/s	Within peak	CDF $\leq$ 0.1 m/s	Within peak	CDF $\leq$ 0.1 m/s	Within peak	CDF $\leq$ 0.1 m/s	Within peak	CDF $\leq$ 0.1 m/s	Within peak
LC-RBPF [7]	76.2%	58.9%	75.1%	48.8%	64.5%	37.3%	64.3%	50.5%	75.6%	66.2%	81.9%	64.8%
TC-RBPF	**79.1%**	**71.9%**	**81.4%**	**54.4%**	**67.7%**	**50.8%**	**71.6%**	**67.5%**	**79.5%**	**71.4%**	**85.8%**	**76.2%**

focusing on the proportion below 0.1 m/s. Although this metric reflects the overall accuracy using the mean velocity of the particles, it does not fully capture how well the particles represent the true motion. Therefore, the probability that at least one particle lies within 0.05 m of the ground truth position was also evaluated, based on the observation that the AFV peak generally appears within this range (see Fig. 2). This metric provides a more direct measure of whether the transition step successfully distributes the particles around the true position. Finally, the position estimation accuracy was evaluated using the CDF of position errors, with a threshold of 0.3 m.

The state-transition performance of the PF was compared between the proposed TC-RBPF and the LC-RBPF, while position estimation was compared across four methods: RTKLIB 2.4.3 [9], rtklibexplorer demo5 [35], LC-RBPF, and the proposed TC-RBPF. RTKLIB is a widely used baseline implementation, and rtklibexplorer extends it with enhanced ambiguity resolution and multipath handling for urban scenarios. The ambiguity resolution mode was set to fix-and-hold for both RTK-GNSS based methods. For all methods, the elevation mask and C/N0 mask were set to 15 degrees and 35 dB-Hz, respectively. Both TC-RBPF and LC-RBPF utilize the same weighting model from [33] in the velocity estimation step to ensure a fair algorithmic evaluation, while RTKLIB and rtklibexplorer were benchmarked using their default settings. The number of particles used in both the LC-RBPF and TC-RBPF was set to 2000. Ground truth data were obtained from a high-precision GNSS/INS reference system, POS LV.

B. Results

1) State transition performance: The evaluation results for the state transition performance are summarized in Table I. The proposed TC-RBPF consistently improves the velocity CDF across all six test environments, although the gain is limited to a few percentage points due to the averaging over 2000 particles. In contrast, the AFV-based metric shows a more substantial improvement in all scenarios, indicating that the proposed transition model more effectively propagates particles toward the true state. The improvement is particularly notable in Nagoya Run3, the most challenging environment among the six, and Tokyo Run1, where severe signal obstruction and multipath effects are present. These results demonstrate that the proposed method enhances not only the overall velocity estimation accuracy but also the spatial coverage and robustness of particle distribution in challenging urban environments. The improvement is primarily due to the direct use of raw Doppler measurements and exclusion of NLOS measurements in the robust KF, which together enable more accurate velocity updates and allow the transition model to better capture the motion dynamics, particularly under degraded GNSS conditions.

2) Position estimation accuracy: The position estimation results are presented in Table II. As summarized in Table II, the proposed method outperforms the three baselines in five out of six environments in terms of the proportion of position errors below 0.3 m. Although rtklibexplorer achieves the highest accuracy in Nagoya Run1, its performance degrades significantly in environments with severe multipath and satellite occlusion. In contrast, the proposed method maintains consistently high accuracy across all test runs. Notably, in Nagoya Run3, the most difficult environment among the six, the proposed method achieves 52.2% below the 0.3 m threshold, outperforming rtklibexplorer by nearly 30 percentage points.

To visually demonstrate the stability and robustness quantified in Table II, Fig. 4 presents time series plots for the two most challenging and representative environments, Nagoya

IEEE Robotics and Automation Letters (RA-L) paper, presented at ICRA 2026, Vienna, Austria. Cite as RA-L paper.

TABLE II
POSITION ESTIMATION ACCURACY COMPARISON OF EACH METHOD ACROSS SIX TEST RUNS.

Method	Nagoya Run1 CDF $\leq$ 0.3 m	Nagoya Run2 CDF $\leq$ 0.3 m	Nagoya Run3 CDF $\leq$ 0.3 m	Tokyo Run1 CDF $\leq$ 0.3 m	Tokyo Run2 CDF $\leq$ 0.3 m	Tokyo Run3 CDF $\leq$ 0.3 m
RTKLIB [9]	53.4%	52.5%	15.2%	27.1%	66.8%	67.7%
rtklibexplorer [35]	**82.7%**	52.3%	22.6%	43.9%	63.9%	68.0%
LC-RBPF [7]	58.8%	49.7%	40.2%	52.0%	66.5%	66.2%
TC-RBPF	71.8%	**54.9%**	**52.2%**	**69.6%**	**71.9%**	**78.2%**

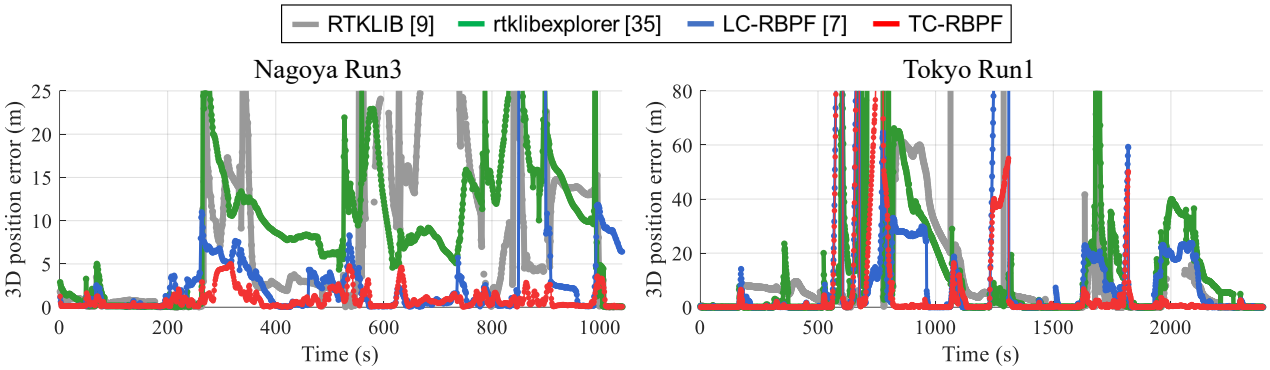

Fig. 4. Time series of 3D position error in two representative environments: Nagoya Run3 and Tokyo Run1. Gray: RTKLIB, green: rtklibexplorer, blue: LC-RBPF, red: proposed TC-RBPF. The proposed method exhibits a consistently lower error envelope and fewer large spikes than the baselines.

TABLE III
ABLATION STUDY RESULTS IN NAGOYA RUN3.

Method	State Transition (Within peak %)	Position (CDF $\leq$ 0.3 m %)
LC-RBPF	37.3%	40.2%
TC-RBPF (Base)	47.3%	45.8%
+ NLOS Rejection	48.6%	46.7%
+ Robust KF	49.2%	49.3%
+ NLOS Rejection & Robust KF	**50.8%**	**52.2%**

Run3 and Tokyo Run1. Across both runs, the baseline methods frequently lose fix or exhibit sudden error jumps, whereas the proposed method maintains a highly stable and accurate trajectory. Even under degraded GNSS conditions, it sustains submeter accuracy for most epochs. However, occasional spikes in the proposed method only occur during brief complete signal outages when RTK-GNSS baselines provide no solution. Without a measurement update in the KF, the particles drift from the true position, producing large temporal errors. Nevertheless, these results confirm that the proposed approach not only improves accuracy, but also ensures robustness against GNSS degradation, making it well-suited for real-world urban navigation applications.

3) Ablation study: To clarify the contribution of each component to the improved performance of the TC-RBPF, we carried out an ablation study using the Nagoya Run3 dataset, which is the most challenging environment. The results are summarized in Table III. This analysis confirms that the TC framework is the primary driver of improvement: TC-RBPF alone yields a 10.0% gain in velocity and 5.6% in position over the LC-RBPF. The Student's t distribution-based robust KF is more effective individually as it mitigates velocity outliers regardless of particle position. In contrast, NLOS rejection works reliably only when particles already cluster near the true position. In the full method, robust KF ensures that particles are clustered more reliably near the true position. This enhances the accuracy of the DD pseudorange residual-based NLOS satellite identification, which in turn further improves state transition performance. Consequently, the full model achieves the most accurate position estimates.

C. Discussion

The proposed TC-RBPF achieved high-accuracy positioning in challenging urban environments, outperforming conventional methods. Despite estimating more state variables than the LC-RBPF, its computational cost remained practical: under 100 ms per epoch without GPU acceleration on a standard CPU (Intel Core i7-10700K, 64 GB RAM). This confirms its suitability for real-time applications.

In the Nagoya Run1 scenario, the accuracy was slightly lower than rtklibexplorer, due to the full GNSS outages in tunnels and underpasses. Since TC-RBPF relies on Doppler-based velocity estimation, the absence of observations hinders reliable state transition and likelihood updates, leading to temporary degradation. Nevertheless, the method achieves centimeter-level accuracy without explicit ambiguity resolution, relying solely on the AFV metric. This shows its effectiveness as a robust alternative to RTK-GNSS in urban environments. While integration with additional sensors such as INS could enhance performance in a GNSS-denied environment, this remains promising for future work. For instance, replacing the KF for velocity estimation with factor graph optimization (FGO) could enable a more robust tight

IEEE Robotics and Automation Letters (RA-L) paper, presented at ICRA 2026, Vienna, Austria. Cite as RA-L paper.

integration with INS. Furthermore, integrating environmental sensors such as cameras and using learning-based models to refine the likelihood calculation or enable intelligent satellite selection may lead to even higher positioning accuracy.

V. Conclusion

This paper proposed a TC-RBPF for GNSS positioning that does not require carrier-phase integer ambiguity resolution. Building upon previous work on LC-RBPF, the proposed method enhances position estimation accuracy by improving the state transition model through tight coupling. In addition, a robust KF based on the Student's t-distribution is introduced to accommodate the heavy-tailed nature of GNSS errors. Furthermore, the proposed method performs particle-wise NLOS rejection using DD pseudorange residuals, dynamically excluding NLOS measurements.

To evaluate the effectiveness of the proposed method, experiments were conducted using the PPC dataset in six urban environments. The results demonstrated that the proposed TC-RBPF achieved significantly higher velocity estimation accuracy compared to the LC-RBPF, even in challenging urban scenarios. This improvement in velocity estimates enhanced the reliability of the PF state transition and enabled high-accuracy real-time positioning without requiring ambiguity resolution.

References

[1] J. Ziegler, P. Bender, M. Schreiber, H. Lategahn, T. Strauss, C. Stiller, T. Dang, U. Franke, N. Appenrodt, C. G. Keller *et al.*, "Making bertha drive—an autonomous journey on a historic route," *IEEE Intelligent transportation systems magazine*, vol. 6, no. 2, pp. 8–20, 2014.

[2] P. D. Groves, Z. Jiang, M. Rudi, and P. Strode, "A Portfolio Approach to NLOS and Multipath Mitigation in Dense Urban Areas," in *26th International Technical Meeting of the Satellite Division of the Institute of Navigation, ION GNSS 2013*, vol. 4, 2013, pp. 3231–3247.

[3] P. J. Teunissen and O. Montenbruck, *Springer handbook of global navigation satellite systems*. Springer, 2017, vol. 10.

[4] D. Kim and R. B. Langley, "Gps ambiguity resolution and validation: methodologies, trends and issues," in *Proceedings of the 7th GNSS Workshop–International Symposium on GPS/GNSS, Seoul, Korea*, vol. 30, no. 2.12, 2000.

[5] T. Suzuki, "Multiple Update Particle Filter: Position Estimation by Combining GNSS Pseudorange and Carrier Phase Observations," in *2024 IEEE International Conference on Robotics and Automation (ICRA)*, 2024, pp. 13 680–13 686.

[6] L. Serrano, D. Kim, R. B. Langley, K. Itani, and M. Ueno, "A GPS velocity sensor: How accurate can it be? - A first look," in *Proceedings of the National Technical Meeting, Institute of Navigation*, vol. 2004, 2004, pp. 875–885.

[7] D. Niimi, A. Fujino, T. Suzuki, and J. Meguro, "Robust position estimation by rao-blackwellized particle filter without integer ambiguity resolution in urban environments," in *2025 IEEE/ION Position, Location and Navigation Symposium (PLANS)*, 2025, pp. 1239–1246.

[8] P. J. Teunissen, "Least-squares estimation of the integer gps ambiguities," in *Invited lecture, section IV theory and methodology, IAG general meeting, Beijing, China*, 1993, pp. 1–16.

[9] T. Takasu and A. Yasuda, "Development of the low-cost RTK-GPS receiver with an open source program package RTKLIB," in *Proc. of The International Symposium on GPS/GNSS*, Jeju, Korea, 2009.

[10] A. Takanose, Y. Atsumi, K. Takikawa, and J. Meguro, "Improvement of reliability determination performance of real time kinematic solutions using height trajectory," *Sensors*, vol. 21, no. 2, 2021. [Online]. Available: https://www.mdpi.com/1424-8220/21/2/657

[11] P. J. Teunissen, "An optimality property of the integer least-squares estimator," *Journal of geodesy*, vol. 73, no. 11, pp. 587–593, 1999.

[12] A. Brack, "Partial ambiguity resolution for reliable gnss positioning—a useful tool?" in *2016 IEEE Aerospace Conference*. IEEE, 2016, pp. 1–7.

[13] J. Zidan, E. I. Adegoke, E. Kampert, S. A. Birrell, C. R. Ford, and M. D. Higgins, "Gnss vulnerabilities and existing solutions: A review of the literature," *IEEE Access*, vol. 9, pp. 153 960–153 976, 2020.

[14] C. C. Counselman and S. A. Gourevitch, "Miniature interferometer terminals for earth surveying: ambiguity and multipath with global positioning system," *IEEE Transactions on Geoscience and Remote Sensing*, no. 4, pp. 244–252, 1981.

[15] S. Cellmer, P. Wielgosz, and Z. Rzepecka, "Modified ambiguity function approach for GPS carrier phase positioning," *Journal of Geodesy*, vol. 84, pp. 267–275, 2010.

[16] S. Cellmer, "A graphic representation of the necessary condition for the mafa method," *IEEE transactions on geoscience and remote sensing*, vol. 50, no. 2, pp. 482–488, 2011.

[17] S. Cellmer, "Search procedure for improving modified ambiguity function approach," *Survey Review*, vol. 45, no. 332, pp. 380–385, 2013.

[18] A. Doucet, N. J. Gordon, and V. Krishnamurthy, "Particle filters for state estimation of jump Markov linear systems," *IEEE Transactions on signal processing*, vol. 49, no. 3, pp. 613–624, 2001.

[19] T. Schon, F. Gustafsson, and P.-J. Nordlund, "Marginalized particle filters for mixed linear/nonlinear state-space models," *IEEE Transactions on Signal Processing*, vol. 53, no. 7, pp. 2279–2289, 2005.

[20] F. Gustafsson, "Particle filter theory and practice with positioning applications," *IEEE Aerospace and Electronic Systems Magazine*, vol. 25, no. 7, pp. 53–82, 2010.

[21] A. Doucet, A. M. Johansen *et al.*, "A tutorial on particle filtering and smoothing: Fifteen years later," *Handbook of nonlinear filtering*, vol. 12, no. 656-704, p. 3, 2009.

[22] F. Mustiere, M. Bolic, and M. Bouchard, "Rao-blackwellised particle filters: examples of applications," in *2006 Canadian Conference on Electrical and Computer Engineering*. IEEE, 2006, pp. 1196–1200.

[23] S. Thrun, W. Burgard, and D. Fox, *Probabilistic Robotics*. MA, Cambridge: MIT Press, 2005.

[24] K. Murphy and S. Russell, "Rao-Blackwellised particle filtering for dynamic Bayesian networks," in *Sequential Monte Carlo methods in practice*. Springer, 2001, pp. 499–515.

[25] M. Montemerlo, S. Thrun, D. Koller, B. Wegbreit *et al.*, "FastSLAM 2.0: An improved particle filtering algorithm for simultaneous localization and mapping that provably converges," in *IJCAI*, vol. 3, no. 2003. Citeseer, 2003, pp. 1151–1156.

[26] A. Giremus, A. Doucet, V. Calmettes, and J.-Y. Tourneret, "A Rao-Blackwellized particle filter for INS/GPS integration," in *2004 IEEE International Conference on Acoustics, Speech, and Signal Processing*, vol. 3, 2004, pp. iii–964.

[27] S. Gupta, A. Mohanty, and G. Gao, "Getting the best of particle and Kalman filters: GNSS sensor fusion using rao-blackwellized particle filter," in *Proceedings of the 35th International Technical Meeting of the Satellite Division of The Institute of Navigation (ION GNSS+ 2022)*, 2022, pp. 1610–1623.

[28] T. Suzuki, "Integration of GNSS positioning and 3D map using particle filter," in *Proceedings of the 29th International Technical Meeting of the Satellite Division of The Institute of Navigation (ION GNSS+ 2016)*, 2016, pp. 1296–1304.

[29] T. Suzuki, "Mobile robot localization with GNSS multipath detection using pseudorange residuals," *Advanced Robotics*, vol. 33, no. 12, pp. 602–613, 2019.

[30] Q. Zhong and P. D. Groves, "Multi-epoch 3d-mapping-aided positioning using bayesian filtering techniques," *NAVIGATION: Journal of the Institute of Navigation*, vol. 69, no. 2, 2022.

[31] Y. Huang, Y. Zhang, N. Li, Z. Wu, and J. A. Chambers, "A novel robust student's t-based kalman filter," *IEEE Transactions on Aerospace and Electronic Systems*, vol. 53, no. 3, pp. 1545–1554, 2017.

[32] F. Tronarp, T. Karvonen, and S. Särkkä, "Student's t-filters for noise scale estimation," *IEEE Signal Processing Letters*, vol. 26, no. 2, pp. 352–356, 2019.

[33] A. Herrera Olmo, H. Suhandri, E. Realini, M. Reguzzoni, and M. C. d. Lacy, "gogps: open-source matlab software," *GPS Solutions*, vol. 20, pp. 1–9, 06 2015.

[34] T. Suzuki, "Precise positioning challenge dataset." [Online]. Available: https://github.com/taroz/PPC-Dataset

[35] T. Everett, T. Taylor, D.-K. Lee, and D. M. Akos, "Optimizing the use of rtklib for smartphone-based gnss measurements," *Sensors*, vol. 22, no. 10, 2022.